Available online at www.sciencedirect.com
ScienceDirect
Journal of Power Sources 180 (2008) 283–293
JOURNAL OF POWER SOURCES
www.elsevier.com/locate/jpowsour

Modeling and simulation of the anode in direct ethanol fuels cells

Ruy Sousa Jr. [a,b], Daniela Marques dos Anjos [a,b], Germano Tremiliosi-Filho [a], Ernesto Rafael Gonzalez [a,*], Christophe Coutanceau [b], Eric Sibert [b], Jean-Michel Léger [b], Kouakou Boniface Kokoh [b]

[a] *Instituto de Química de São Carlos, Universidade de São Paulo, Av. Trabalhador Sãocarlense, 400, C. P. 780, 13560-970 São Carlos, SP, Brazil*
[b] *Laboratoire de Catalyse en Chimie Organique, Université de Poitiers, 40, Av. du Recteur Pineau, 86022 Poitiers, France*

Received 10 December 2007; received in revised form 24 January 2008; accepted 24 January 2008
Available online 7 February 2008

Abstract

Mathematical modeling has been extensively applied to the study and development of fuel cells. In this work, the objective is to characterize a mechanistic model for the anode of a direct ethanol fuel cell and perform appropriate simulations.

The software Comsol Multiphysics® (and the Chemical Engineering Module) was used in this work. The software Comsol Multiphysics® is an interactive environment for modeling scientific and engineering applications using partial differential equations (PDEs). Based on the finite element method, it provides speed and accuracy for several applications.

The mechanistic model developed here can supply details of the physical system, such as the concentration profiles of the components within the anode and the coverage of the adsorbed species on the electrode surface. Also, the anode overpotential–current relationship can be obtained. To validate the anode model presented in this paper, experimental data obtained with a single fuel cell operating with an ethanol solution at the anode were used.

Keywords: Fuel cell anode; Ethanol; Mechanistic model; Simulations

1. Introduction

The advantages of fuel cells as clean, silent and efficient power sources have been demonstrated, and proton exchange membrane fuel cells (PEMFCs) are presently among the most promising of these devices [1,2]. Although a PEMFC working with hydrogen presents the highest efficiency and environmental compatibility, hydrogen is not the best choice as a fuel because of the problems of production, storage and distribution. A liquid fuel like a low molecular weight alcohol can be used in a direct alcohol fuel cell, which has the advantage of being a much simpler system. Methanol has been used as fuel with some success, but it has some disadvantages, e.g. it is relatively toxic, inflammable with a low boiling point (65 °C), and it is neither a primary fuel, nor a renewable fuel. Therefore, other alcohols are being considered as alternative fuels. Ethanol is an attractive liquid fuel for direct alcohol fuelled systems. It is the major renewable biofuel obtained from the fermentation of biomass, and ethanol is less toxic than methanol. Wang et al. [3] compared the performance of fuel cells employing an H_3PO_4-doped polybenzimidazole membrane operating on various methanol-alternative fuels. They found that ethanol is a promising alternative fuel with an electrochemical activity comparable to that of methanol.

Several experimental studies on the electro-oxidation of ethanol have been devoted mainly to identifying the adsorbed intermediates on the electrode and elucidating the reaction mechanism by means of various techniques, as differential electrochemical mass spectrometry (DEMS), in situ Fourier transform infrared spectroscopy (FTIRS) and electrochemical thermal desorption mass spectroscopy (ECTDMS) [4–9]. Based on the foregoing work, the global oxidation mechanism of ethanol in acid solution may be summarized by the following scheme of parallel reactions:

$$CH_3CH_2OH \rightarrow [CH_3CH_2OH]_{ad} \rightarrow C1_{ad}, C2_{ad} \rightarrow CO_2 \text{ (total oxidation)} \quad (1)$$

* Corresponding author. Tel.: +55 16 33739899; fax: +55 16 33739952.
E-mail address: ernesto@iqsc.usp.br (E.R. Gonzalez).

0378-7753/$ – see front matter © 2008 Elsevier B.V. All rights reserved.
doi:10.1016/j.jpowsour.2008.01.058

Nomenclature

C_k	species concentration (mol m^{-3})
D_k	diffusivity (m^2 s^{-1})
F	Darcy's drag
j	current density (A m^{-2} or mA cm^{-2})
j_0	constant in Tafel equation (A m^{-2})
$k0$	kinetic constant (m s^{-1})
$k0'$	kinetic constant
$k0''$	kinetic constant (mol m^{-2} s^{-1})
$k1$	kinetic constant (m s^{-1})
$k1'$	kinetic constant
$k4$	kinetic constant (mol m^{-2} s^{-1})
$k4'$	kinetic constant (mol m^{-2} s^{-1})
$k5$	kinetic constant (mol m^{-2} s^{-1})
L	length (m)
R	resistance (Ω m^2) = 0.285×10^{-4} Ω m^2
t	time (s)
u	component of the velocity vector $\vec{u}$ in the x direction (m s^{-1})
$\vec{u}$	velocity vector (m s^{-1})
v	component of the velocity vector $\vec{u}$ in the y direction (m s^{-1})
x	x axis (m)
y	y axis (m)

Greek letters

α	transfer coefficient
Γ	site density (mol m^{-2})
ε	porosity
η	overpotential (V or mV)
θ	coverages of the different species
μ	viscosity (kg m^{-1} s^{-1})
ρ	density (kg m^{-3})

$$CH_3CH_2OH \rightarrow [CH_3CH_2OH]_{ad} \rightarrow CH_3CHO \rightarrow CH_3COOH \text{ (partial oxidation)} \quad (2)$$

The formation of CO_2 is believed to go through two adsorbed intermediates $C1_{ad}$ and $C2_{ad}$, which represent fragments with one and two carbon atoms, respectively. In spite of many advances in the understanding of the mechanism of ethanol oxidation, there are still some unclear aspects. For instance, there is some controversy on whether acetic acid is formed in one step or through the aldehyde. Also, there is no agreement regarding the nature of the adsorbed species. According to some workers, the carbon–carbon bond is preserved, so a larger quantity of intermediates of the type C2 are formed [4,5], but others claim that the main intermediates contain only one carbon atom and are of the type C1 [6,8]. Breaking the C–C bond for a total oxidation to CO_2 is a major problem in ethanol electrocatalysis. Thus, high yields of partial oxidation products, CH_3CHO and CH_3COOH, are found at Pt catalysts [10,11]. These parallel reactions cause a considerable lowering of the fuel capacity to generate electricity and produce undesirable substances. Platinum is at present the best-known catalyst for the adsorption and dissociation of small organic molecules, but it has a limited ability for breaking the C–C bond. In this context, the research objectives in this area have been the search for more effective electrocatalysts, which ideally promote the complete oxidation of ethanol at potentials as low as possible. Presently, research in electrocatalysts is focused on the development of binary and ternary Pt-based materials.

Mathematical modeling has been extensively applied in the study and development of fuel cells [12]. Modeling studies of different physical systems, e.g. usual cathodes and biochemical fuel cells [13], have been developed in this laboratory. In this work, a mechanistic model for an ethanol anode is proposed and appropriate simulations performed, with the objective of providing simulation elements that can help with the understanding of the anodic process in direct ethanol fuel cells.

2. Methodology

Simulations were performed using the software Comsol Multiphysics® [14]. This software is an interactive environment for modeling scientific and engineering systems based on partial differential equations (PDEs). Using the finite element method [15,16], it provides speed and accuracy for multiphysics applications and it covers all the facets of the modeling process. It contains CAD ("Computer Aided Design") tools, interfaces for specifications of equations and physical and chemical parameters, mesh generation, optimized solvers, as well as visualization and post-processing tools.

2.1. Specialized modules

This work was developed using the Chemical Engineering Module [17], which is divided into many application modes.

2.1.1. Momentum balances

The Navier–Stokes equations for fluid flow;
Darcy's Law for porous media flow.

2.1.2. Energy balances

Heat transfer by diffusion, convection and conduction.

2.1.3. Material balances

Convection and diffusion.

In these applications, the physical (and chemical) properties appearing in the equations are specified so the PDEs are formulated.

The modeling procedure using the Chemical Engineering Module is analogous to the general methodology of COMSOL Multiphysics® [18]. It involves the following steps:

1. create or import the geometry in 1D, 2D or 3D;
2. select the equations that define the system;
3. specify the properties or coefficients in the selected equations;
4. set the boundary and initial conditions;

5. generate and refine the finite element mesh;
6. run the simulation;
7. visualize and process the results.

For the validation experiments, the membrane electrode assembly (MEA) was prepared by hot pressing a pretreated Nafion® 117 membrane between a Pt/C (metal loading 30 wt.%) E-TEK cathode (1 mg cm^{-2} Pt) and a $Pt_{0.85}Sn_{0.8}W_{0.7}$/C (metal loading 40 wt.%) anode (1 mg cm^{-2} Pt), at 125 °C for 2 min under a pressure of 35 kg cm^{-2}. The operating fuel cell performance was determined in a single direct ethanol fuel cell (DEFC) with an electrode geometric surface area of 4.6 cm^2. The temperature was set to 90 °C for the fuel cell and 95 °C for the oxygen humidifier. The distribution of reaction products under the DEFC operating conditions was determined at a current of 30 mA cm^{-2}. The final products were trapped on the anode and the products derived from the crossover process were collected on the cathode outlet in an iced flask. A High Performance Liquid Chromatograph (HPLC) using an Aminex HPX-87H column from Bio-Rad with a UV detector SPD-MICA from Shimadzu was used to analyze quantitatively the reaction products at the outlet of both anode and cathode.

3. Results and discussion

Fig. 1 shows the simplified scheme of the fuel cell anode used here. This 2D pattern is usually used to simulate parallel flow fields (interdigitated flow fields, on the other hand, are usually associated with 3D models).

The mathematical model of the ethanol anode is based on material balances considering diffusive and/or convective fluxes $((\partial(C_k))/\partial t) = -\nabla(\vec{u}C_k) + \nabla(\varepsilon D_k \nabla C_k) = 0$ for the species in solution (mainly water, ethanol, acetic acid and acetaldehyde or CO_2). Additionally, the model assumes Fickĭs Law for diffusion and Tafel kinetics coupled to adsorption steps on the catalytic surface. The treatment is similar to that of Nordlund and Lindberg [19] for a methanol anode. Besides Nordlund and Lindberg [19], it is relevant to mention the works of Zhou et al. [20], Sundmacher et al. [21], and Vidakovic et al. [22]. The velocity field was also calculated (according to $((\partial(\rho\vec{u}))/\partial t) = -\nabla(\rho\vec{u}\vec{u}) - \nabla P + \nabla(\mu(\nabla\vec{u} + (\nabla\vec{u})^{\mathrm{T}})) + F$).

Reaction steps on the catalytic surface are the scheme of Eqs. (3a)–(3e). Eq. (3d) represents the formation of the species OH_{ads},

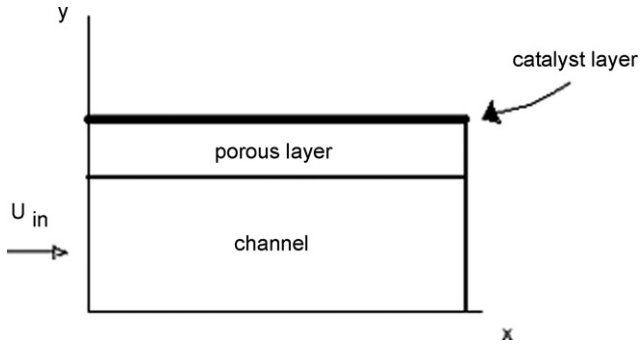

Fig. 1. Scheme of a porous anode.

which plays a very important role in the oxidation of some intermediate species by providing the necessary oxygen atoms. On the real catalyst surface of binary and ternary Pt-based electrocatalysts, there are different sites with different crystal structures available for adsorption and reaction. Small organic molecules will mostly adsorb on Pt. Different sites may present different rate constants, but very detailed information, not available at the moment, is necessary to differentiate them quantitatively. So, we have chosen as a good initial approach to describe the catalyst through one set of rate constants, such as in Nordlund and Lindberg [19].

$$CH_3CH_2OH \leftrightarrow CH_3CHO_{ads} + 2H^+ + 2e^- \qquad k0, k0' \tag{3a}$$

$$CH_3CHO_{ads} \rightarrow CH_3CHO \qquad k0'' \tag{3b}$$

$$CH_3CH_2OH + H_2O \leftrightarrow CH_3CO_{ads} + 2H^+ + 3e^- + H_3O^+ \qquad k1, k1' \tag{3c}$$

$$H_2O \leftrightarrow OH_{ads} + H^+ + e^- \qquad k4, k4' \tag{3d}$$

$$CH_3CO_{ads} + OH_{ads} \rightarrow CH_3COOH \qquad k5 \tag{3e}$$

For the coverages θ of the different species on the catalyst surface, the following steady-state conditions are postulated:

$$\Gamma\frac{d\theta_{CH_3CHO}}{dt} = k0 \cdot C_{CH_3CH_2OH} \cdot (1 - \Sigma\theta) \cdot \exp(0.5 \cdot \text{const.}\,\eta) - k0' \cdot \theta_{CH_3CHO} \cdot \exp(-0.5 \cdot \text{const.}\,\eta) - k0'' \cdot \theta_{CH_3CHO} = 0 \tag{4a}$$

$$\Gamma\frac{d\theta_{CH_3CO}}{dt} = k1 \cdot C_{CH_3CH_2OH} \cdot (1 - \Sigma\theta) \cdot \exp(\alpha 1 \cdot \text{const.}\,\eta) - k1' \cdot \theta_{CH_3CO} \cdot \exp(-(1 - \alpha 1) \cdot \text{const.}\,\eta) - k5 \cdot \theta_{OH} \cdot \theta_{CH_3CO} = 0 \tag{4b}$$

$$\Gamma\frac{d\theta_{OH}}{dt} = k4 \cdot (1 - \Sigma\theta) \cdot \exp(0.5 \cdot \text{const.}\,\eta) - k4' \cdot \theta_{OH} \cdot \exp(-0.5 \cdot \text{const.}\,\eta) - k5 \cdot \theta_{OH} \cdot \theta_{CH_3CO} = 0 \tag{4c}$$

From which the variables θ are obtained as a function of the anode overpotential.

The scheme corresponding to Eqs. (3a)–(3e) is adequate for the electro-oxidation of ethanol on a platinum electrode, where the main pathways lead to the formation of acetaldehyde and acetic acid, so the scheme corresponds to a realistic model.

Because modeling allows to postulate useful, albeit unrealistic pathways for the reaction, an ideal, unrealistic model consisting in the total oxidation process will also be considered as reference:

$$CH_3CH_2OH + 3H_2O \rightarrow 2CO_2 + 12H^+ + 12e^- \tag{5}$$

As boundaries, the following conditions were considered: for $0 < y <$ channel height: velocity components and species con-

centration at channel entrance:

$$u|_{x=0} = u_{\text{in}}, \quad v|_{x=0} = 0$$
$$C_{H_2O}|_{x=0} = 50111\,\text{mol}\,\text{m}^{-3},$$
$$C_{CH_3CH_2OH}|_{x=0} = 2000\,\text{mol}\,\text{m}^{-3},$$
$$C_{CO_2}|_{x=0} = 0 \text{ (no } CO_2 \text{ at channel entrance)}$$

or

$$C_{H_2O}|_{x=0} = 50111\,\text{mol}\,\text{m}^{-3},$$
$$C_{CH_3CH_2OH}|_{x=0} = 2000\,\text{mol}\,\text{m}^{-3},$$
$$C_{\text{acetaldehyde}}|_{x=0} = 0 \text{ (no acetaldehyde at channel entrance)},$$
$$C_{\text{acetic acid}}|_{x=0} = 0 \text{ (no acetic acid at channel entrance)}$$

for channel height $< y <$ total height:

$$u|_{x=0} = 0, \quad v|_{x=0} = 0 \text{ (zero velocity at "wall")},$$
$$\left(\frac{\partial(C_i)}{\partial x}\right)|_{x=0} = 0 \text{ (insulation/symmetry)}$$
$$u|_{x=L} = 0, \quad v|_{x=L} = 0 \text{ (zero velocity at "wall")},$$
$$\left(\frac{\partial(C_i)}{\partial x}\right)|_{x=L} = 0 \text{ (insulation/symmetry)}$$

for $0 < x <$ cell length:

$$u|_{y=0} = 0, \quad v|_{y=0} = 0 \text{ (zero velocity at "wall")},$$
$$\left(\frac{\partial(C_i)}{\partial y}\right)|_{y=0} = 0 \text{ (insulation/symmetry)}$$

for the catalyst interface:

$$-\varepsilon D_k \left(\frac{\partial(C_{H_2O})}{\partial y}\right)|_{y=\text{total height}} = \text{diffusive flux} = \frac{j}{4F}$$
$$= \text{reaction flux}_{\text{specie}_i}$$
$$-\varepsilon D_k \left(\frac{\partial(C_{CH_3CH_2OH})}{\partial y}\right)|_{y=\text{total height}} = \text{diffusive flux}$$
$$= \frac{j}{12F} = \text{reaction flux}_{\text{specie}_i}$$
$$-\varepsilon D_k \left(\frac{\partial(C_{CO_2})}{\partial y}\right)|_{y=\text{total height}} = \text{diffusive flux} = -\frac{j}{6F}$$
$$= \text{reaction flux}_{\text{specie}_i}$$
$$j = j_0 \left(\frac{C_{CH_3CH_2OH}}{C_{CH_3CH_2OH,\text{ref}}}\right)^{0.25} \exp\left(\frac{\alpha_A F \eta}{RT}\right)$$

or

$$\text{diffusive flux}_{\text{specie}_i} = \text{adsorption/reaction flux}_{\text{specie}_i}$$

The operating conditions and the parameters considered are presented in Table 1.

A finite element mesh of 75×17 elements was used in the simulations when considering the ideal model and a mesh of 80×17 elements was used when considering the realistic model. In the x "along-channel" direction (see Fig. 1), around 100 grid-points are typically required. We used 75 (ideal model) and 80 (realistic model). Besides, 6–10 grid-points are needed to sufficiently resolve each of the distinctive regions "through-plane" (y direction; channel, diffusion, membrane...). We used 10 (channel) + 7 (diffusion). So, we used very typical values. Considering the reference model, that is the total oxidation process, Figs. 2–4 show the concentration profiles for the species in solution at an anode overpotential of 0.37 V and the conditions given in

Table 1
Parameters used in the modeling

Water diffusivity (in liquid phase)	D_{H_2O}	$5 \times 10^{-10}\,\text{m}^2\,\text{s}^{-1}$	Ref. [23]
Ethanol diffusivity (in liquid phase)	$D_{CH_3CH_2OH}$	$6 \times 10^{-9}\,\text{m}^2\,\text{s}^{-1}$	Ref. [23]
CO_2 diffusivity (in liquid phase)	D_{CO_2}	$8 \times 10^{-9}\,\text{m}^2\,\text{s}^{-1}$	Ref. [23]
Acetaldehyde diffusivity (in liquid phase)	D_{CH_3CHO}	$6 \times 10^{-9}\,\text{m}^2\,\text{s}^{-1}$	Assumed (equal to D_{CH_3COOH})
Acetic acid diffusivity (in liquid phase)	D_{CH_3COOH}	$6 \times 10^{-9}\,\text{m}^2\,\text{s}^{-1}$	Ref. [23]
Diffusion layer porosity	ε	0.9 (typical value) or 1 (in the simulations considering the ideal model)	
Tafel equation constant (ethanol, ideal model)	j_0	$68.33 \times 10^{-1}\,\text{A}\,\text{m}^{-2}$	Ref. [24]
Ethanol reference concentration (ideal model)	$C_{CH_3CH_2OH,\text{ref}}$	$500\,\text{mol}\,\text{m}^{-3}$	Ref. [24]
Anode transfer coefficient (ethanol, ideal model)	α_A	0.48	Ref. [24]
Kinetic constant	$k0$	$3 \times 10^{-6}\,\text{m}\,\text{s}^{-1}$	Assumed
Kinetic constant	$k0'$	0	Reaction (3a) considered irreversible
Kinetic constant	$k0''$	$1 \times 10^{-2}\,\text{mol}\,\text{m}^{-2}\,\text{s}^{-1}$	Ref. [25]
Kinetic constant	$k1$	$7 \times 10^{-8}\,\text{m}\,\text{s}^{-1}$	Assumed
Kinetic constant	$k1'$	0	Reaction (3c) considered irreversible
Coefficient	$\alpha 1$	0.8	Assumed
Kinetic constant	$k4$	$1 \times 10^{-5}\,\text{mol}\,\text{m}^{-2}\,\text{s}^{-1}$	Ref. [22]
Kinetic constant	$k4'$	$1\,\text{mol}\,\text{m}^{-2}\,\text{s}^{-1}$	Ref. [22]
Kinetic constant	$k5$	$1 \times 10^{-1}\,\text{mol}\,\text{m}^{-2}\,\text{s}^{-1}$	Assumed
Channel height		0.0008 m	Measured
Diffusion layer height		0.0004 m	Typical value
Anode length	L	0.0215 m	Measured
Temperature	T	90 °C (363 K)	Measured

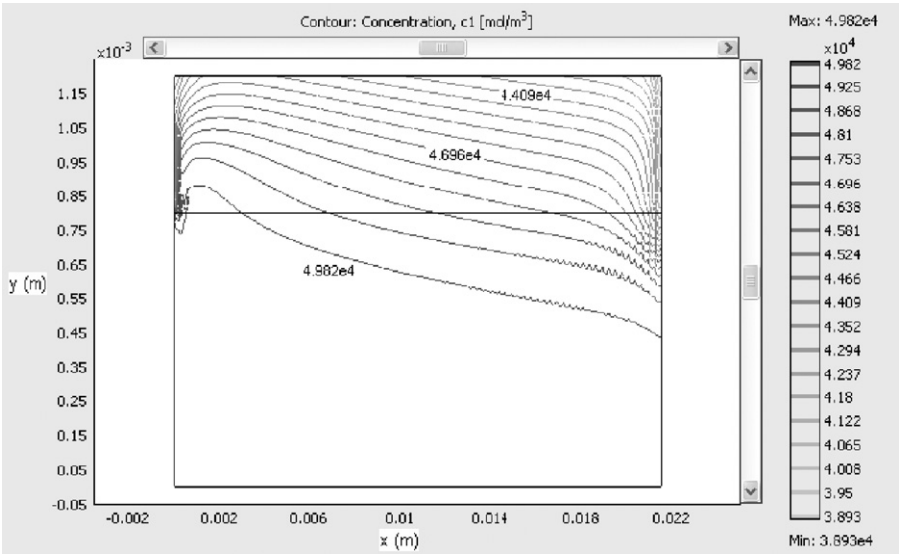

Fig. 2. Water concentration profile for the reference model.

Table 1. Water consumption can be seen in Fig. 2, but the concentration does not become too low in any place. The shape of the curves reveals the effect of a predominantly convective flux in the channels and a mainly diffusive flux in the porous layer. Finally, Fig. 5 shows the overpotential–current curve that results for the ideal model.

Considering now the realistic model, Figs. 6–9 show the concentration profiles at an anode overpotential of 0.37 V. When comparing Figs. 2 and 6, it is observed that water concentration close to catalyst surface is larger for the realistic model. This is correct, because in the real situation less water is consumed. The ideal model predicts higher current densities, which corresponds to higher water consumption. When comparing Figs. 3 and 7, it is observed almost the same consumption of ethanol, but as will be seen in Fig. 11, the current density for the realistic model will be lower.

Fig. 10 shows the coverages of the adsorbed intermediate species postulated in Eqs. (3a)–(3e), as a function of the overpotential. The results show that at an overpotential around 0.41 V, the surface coverage of OH starts being larger than the surface coverage of CH_3CO. Finally, Fig. 11 shows the overpotential–current plot for the realistic model compared with that obtained for the ideal model. It can be seen that at higher overpotentials (over 0.44 V), the increasing OH coverage decreases the cell performance. When this non-Tafel behaviour is observed, it means that adsorbed hydroxide can compete with the adsorption of other species. Nevertheless, it is important to notice that a model which describes the catalytic reaction

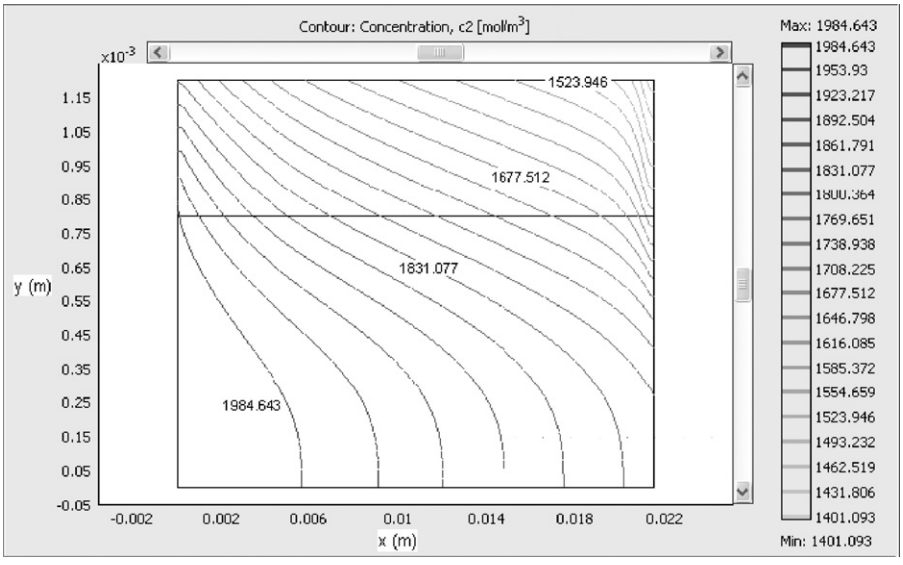

Fig. 3. Ethanol concentration profile for the reference model.

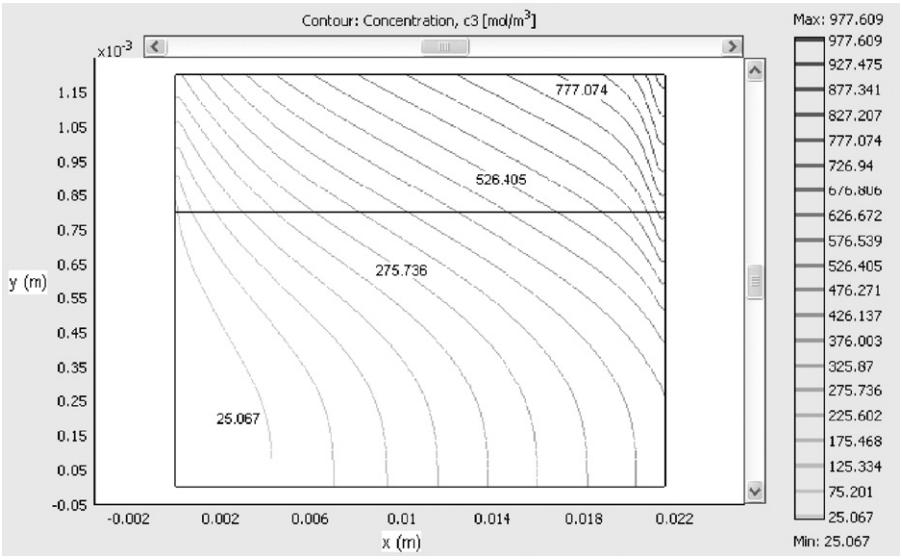

Fig. 4. CO_2 concentration profile for the reference model.

through one set of rate constants (adsorption on the same type of site), such as in this paper and in Nordlund and Lindberg [19], that kind of behaviour (competition) can be "favoured". So, if the non-Tafel behaviour is not observed, a more rigorous model, with a more complex description of adsorption sites can improve the modeling predictions at high overpotentials. However, as mentioned above, very detailed information is necessary to differentiate rate constants for different sites.

To validate the anode model presented in this paper, experimental data from this laboratory obtained with a single cell operating with an ethanol anode and a serpentine flow field were used. Since a serpentine flow field was used, we considered the scheme in Fig. 1 to model the flow path as a sequence of four flow steps (three U-turn regions not affecting the concentration profiles, only changing the flow direction), extending the modeling approach. An oxygen cathode (at 3 atm) and a Nafion® 117 membrane completed the system (see Fig. 12). It is important to notice that the model is still 2D, with one x "along-channel" dimension, one y "through-plane" dimension and no dimension in the direction perpendicular to the xy plane, because the effect of the U-turn on the flow and concentration pattern was not considered [26]. That seems to be the only possible way of considering a 2D approach for the problem, because the along-channel x direction and the through-plane y direction are the more important and cannot be omitted. However, a complete modeling approach must always be 3D (but 3D models require additional computer capabilities).

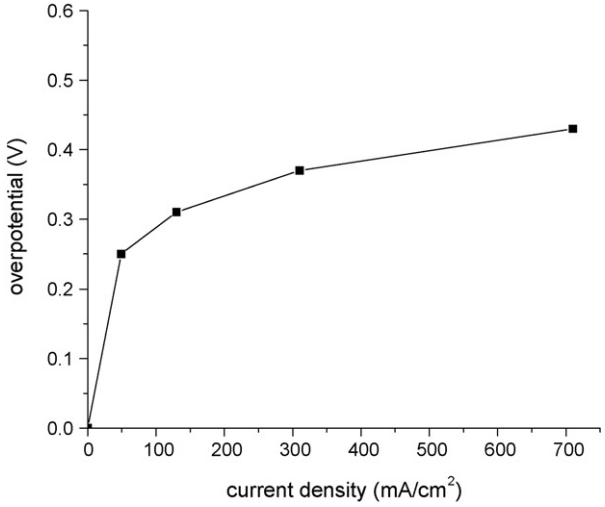

Fig. 5. Overpotential–current plot for the reference model.

A standard mathematical model of a cathode was considered. It is based on species balance equations. Other considerations are: steady-state operation, Fick's diffusion mechanism and Tafel kinetics. Regarding the Nafion® membrane, it was modeled as permeable, in a sense that crossover is permitted. Of course, the inclusion of the membrane and the crossover process will result in a distribution of species not only within the anode, but also in the whole cell and particularly at the cathode. The standard parameters considered to model the cathode are presented in Table 2.

The experiments with the single cell were done at a current density of 300 A m^{-2} (30 mA cm^{-2}).

Table 2
Parameters considered to model the cathode

Oxygen diffusivity	D_{O_2}	0.08×10^{-4} m^2 s^{-1}
Diffusion layer porosity	ε	0.9
Constant in Tafel equation	$j_0/C_{O_2,ref}$	0.0064 A m mol^{-1}
Cathode transfer coefficient	α_C	2
Channel height		0.0008 m
Gas diffusion layer height		0.0004 m
Cathode length	L	0.0215 m

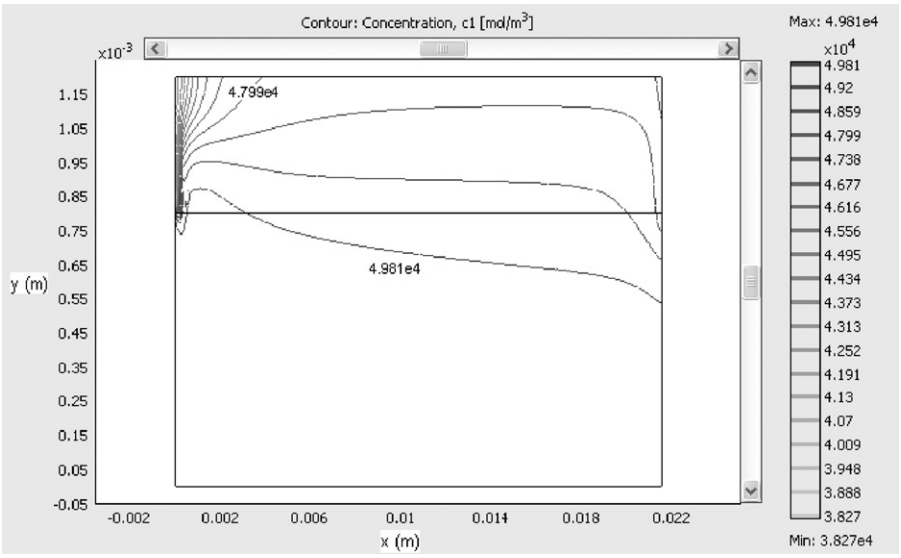

Fig. 6. Water concentration profile for the realistic model.

The results in terms of the concentrations of the product species (ethanol concentration was not measured) were

at the ANODE channel exit:
acetic acid = 7 mol m^{-3}
acetaldehyde = 8 mol m^{-3},

at the CATHODE channel exit:
acetic acid = 59 mol m^{-3}
acetaldehyde = 31 mol m^{-3}.

Figs. 13a, b and 14a, b show the simulation results at a current density of 290 A m^{-2} (29 mA cm^{-2}), in terms of the concentration profiles of acetic acid and acetaldehyde at the anode and cathode exits.

The simulated average acetic acid and acetaldehyde concentrations at the anode channel exit were 6 and 9 mol m^{-3}, respectively. Average acetic acid and acetaldehyde concentrations at the cathode channel exit were 20 and 66 mol m^{-3}, respectively. So, it may be concluded that there is a good agreement between the experimental and the simulated results for the current density, the cell potential ($V = 0.85 - \eta_{anode} + \eta_{cathode} - R_j$) and the concentrations of product species at the anode. On the other hand, there is obviously some disagreement regarding the concentrations of product species at the cathode. The experimental results show that acetaldehyde concentration at the cathode is smaller than

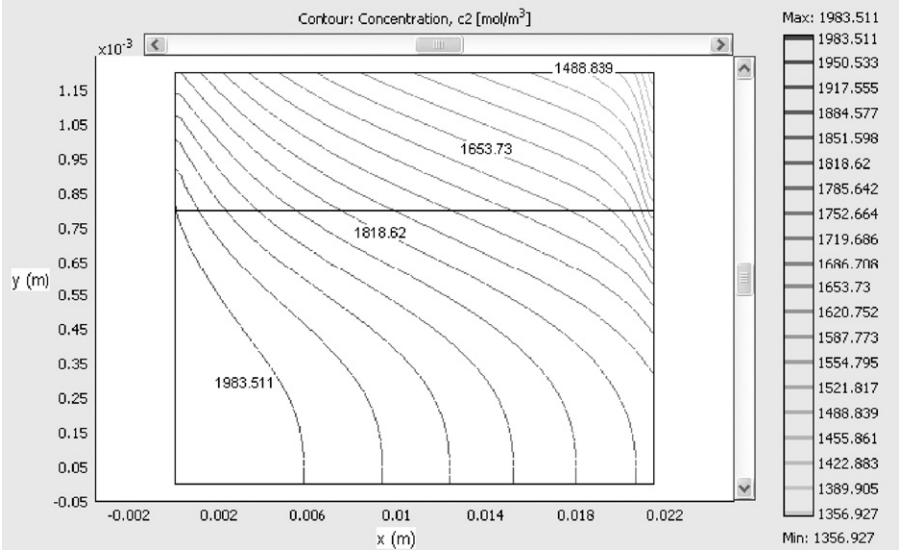

Fig. 7. Ethanol concentration profile for the realistic model.

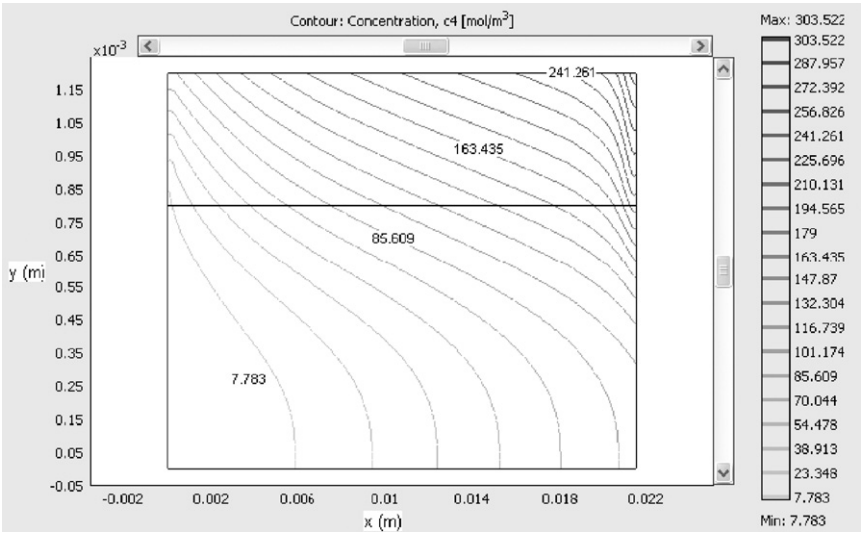

Fig. 8. Acetic acid concentration profile for the realistic model.

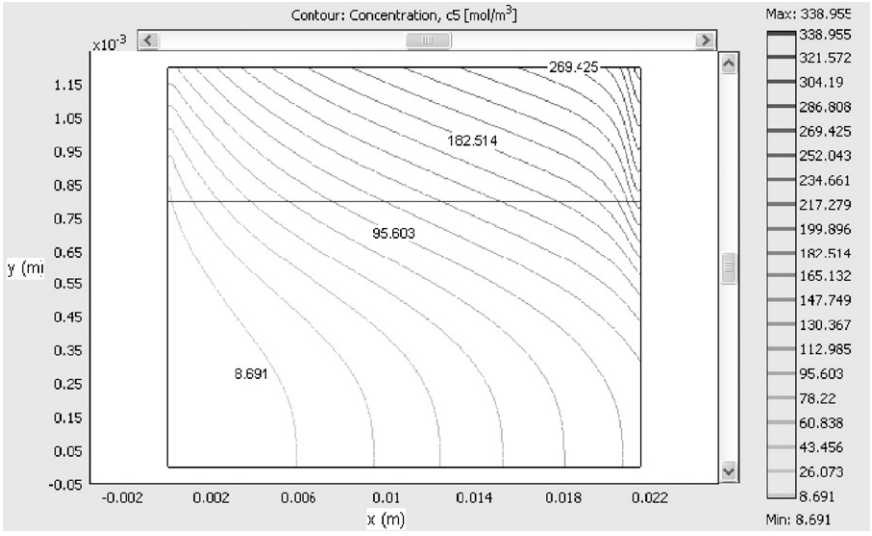

Fig. 9. Acetaldehyde concentration profile for the realistic model.

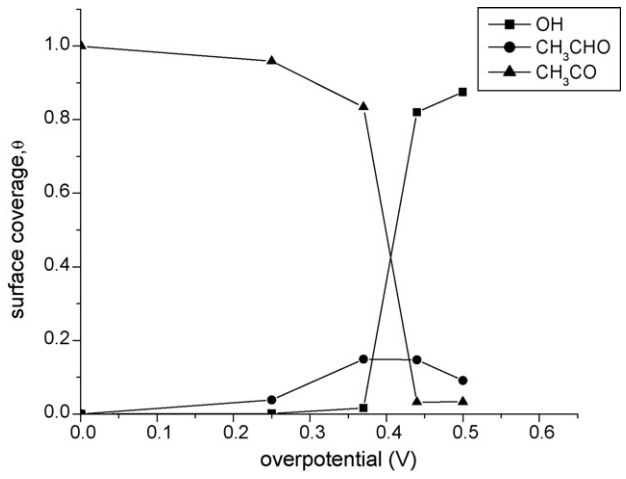

Fig. 10. Coverages of the adsorbed species on the catalyst surface as a function of the anode overpotential for the realistic model.

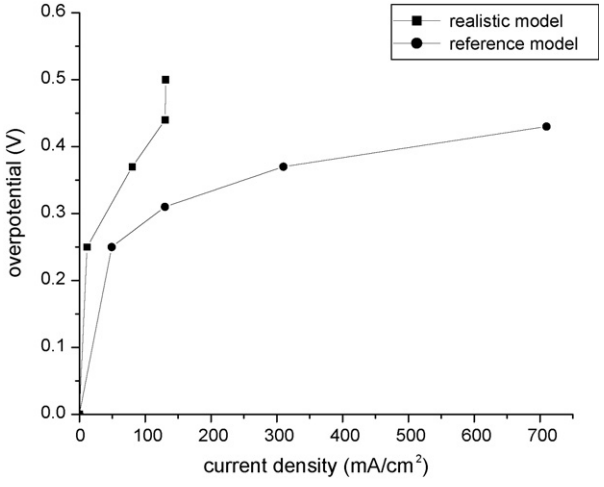

Fig. 11. Overpotential–current plot for the realistic model compared with the reference model.

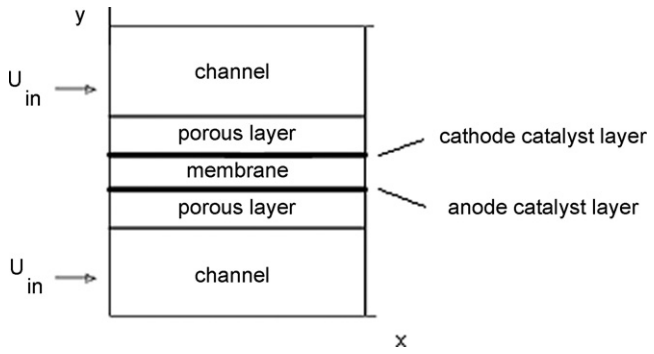

Fig. 12. Scheme of a unitary cell.

the simulated value, while the concentration of acetic acid is larger than the simulated value. This can be understood if it is considered that in the experiments some acetaldehyde may have been lost by evaporation, because of its high volatility, and also that some acetaldehyde may have been oxidized to acetic acid.

Finally, experimental data from this laboratory (fuel cell potential vs. current density, with the same ternary anode) were used to carry out a comparison between experimental and modeling results for a complete polarization curve, as shown in Fig. 15. Again, a good agreement between model predictions and experimental results was obtained. It is important to mention that the comparison of modeling with experimental results for the fuel cell is in the operational (anode) overpotential range, which is below 0.44 V (and below the non-Tafel behaviour region mentioned above). Fig. 16 shows separately the anode and cathode overpotentials.

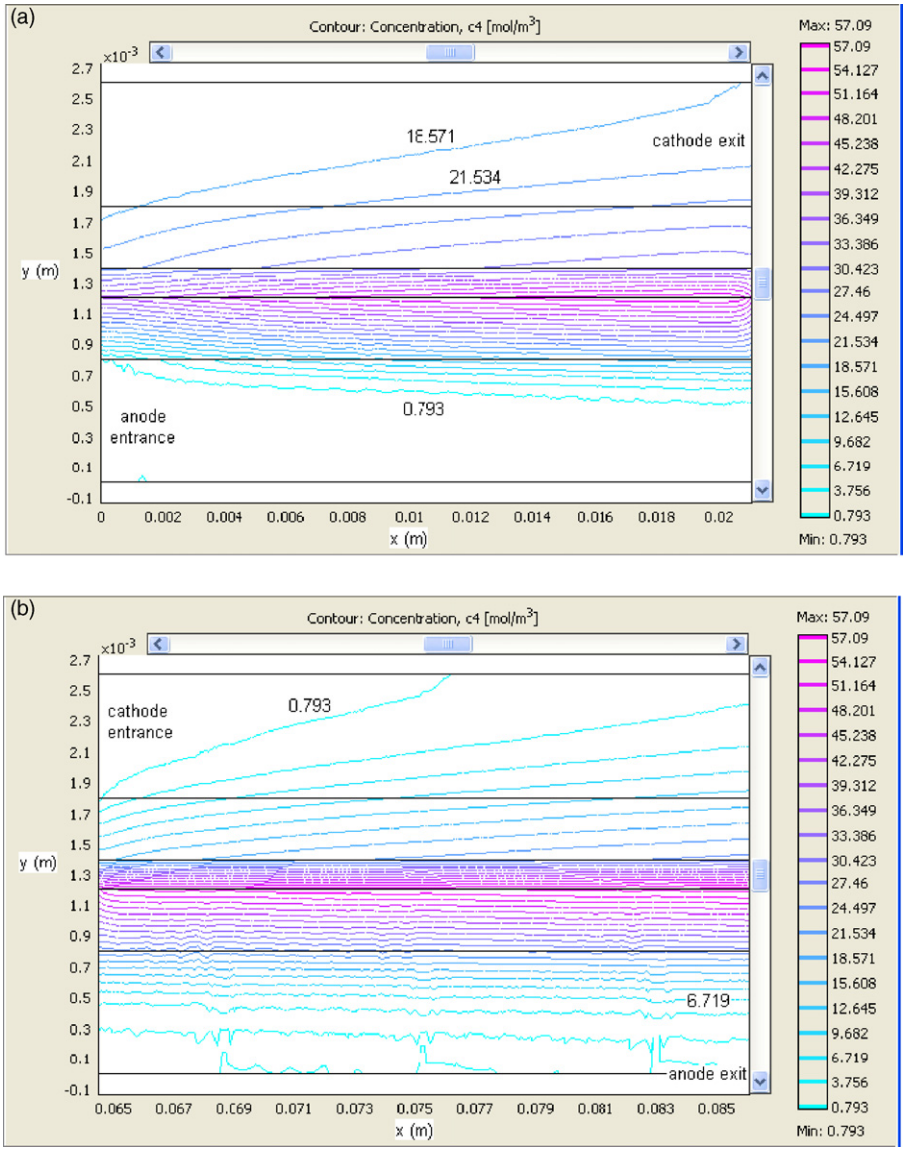

Fig. 13. (a) Simulation of a unitary cell operating with an ethanol anode (acetic acid concentration profile—cathode exit). (b) Simulation of a unitary cell operating with an ethanol anode (acetic acid concentration profile—anode exit).

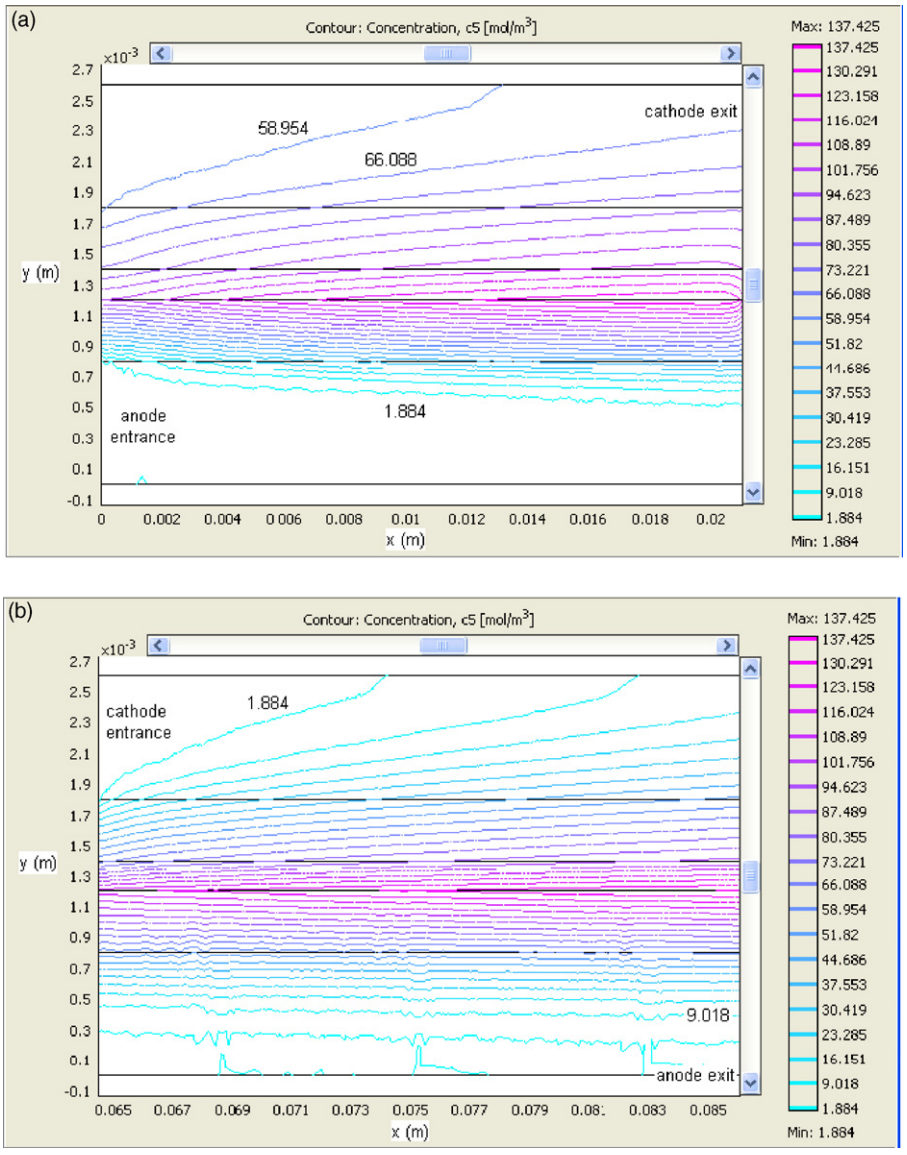

Fig. 14. (a) Simulation of a unitary cell operating with an ethanol anode (acetaldehyde concentration profile—cathode exit). (b) Simulation of a unitary cell operating with an ethanol anode (acetaldehyde concentration profile—anode exit).

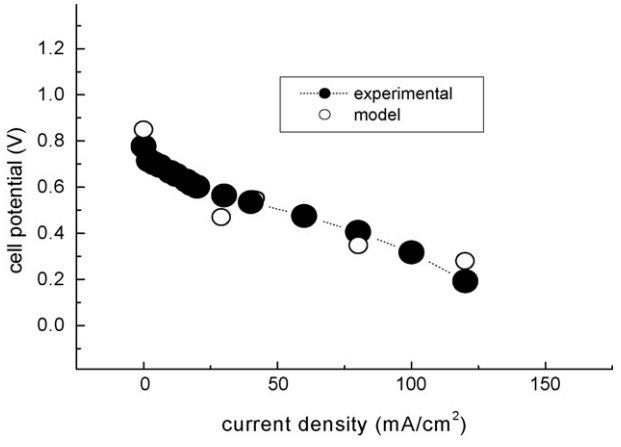

Fig. 15. Fuel cell potential vs. current density.

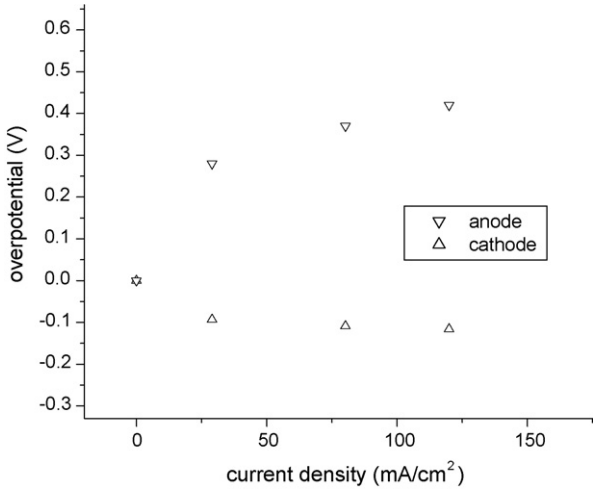

Fig. 16. Anode and cathode overpotentials.

4. Conclusions

A mechanistic model for the anode of a direct ethanol fuel cell was developed on the basis of a realistic mechanism for the reaction that considers the formation of acetaldehyde and acetic acid among the products. From the model, it was possible to get details of the physical system, such as the concentration profiles of the components within the diffusion anode and the coverage of the adsorbed species on the electrode surface.

The model allowed to obtain the overpotential vs. current plot. At all overpotentials, the currents are lower than those that would be obtained with an ideal model that considers the total oxidation to CO_2.

The concentrations of acetaldehyde and acetic acid at the anode, due to the oxidation reaction, and at the cathode, due to crossover, showed good agreement with those determined experimentally in a single direct ethanol fuel cell. Finally, the comparison between experimental data from this laboratory (fuel cell potential vs. current density) and modeling results showed good agreement, giving support to the procedures employed here.

Acknowledgements

The authors thank the CAPES-COFECUB collaboration project No. 498/05 between the Laboratoire de Catalyse en Chimie Organique of the Université de Poitiers, France, and the Instituto de Química de São Carlos, USP, Brazil. Thanks are also due to FAPESP, Brazil.

References

[1] K.B. Prater, J. Power Sources 61 (1996) 105.
[2] C. Stone, A.E. Morrison, Solid State Ionics 152 (2002) 1.
[3] J. Wang, S. Wasmus, R.F. Savinell, J. Electrochem. Soc. 142 (1995) 4218.
[4] J. Willsau, J. Heitbaum, J. Electroanal. Chem. 194 (1985) 27.
[5] T. Iwasita, E. Pastor, Electrochim. Acta 39 (1994) 531.
[6] B. Bittins-Cattaneo, S. Wilhelm, E. Cattaneo, H.W. Buschmann, W. Vielstich, Ber. Bunsenges, Phys. Chem. 92 (1988) 1210.
[7] H. Hitmi, E.M. Belgsir, J.-M. Leger, C. Lamy, R.O. Lezna, Electrochim. Acta 39 (1994) 407.
[8] J.F.E. Gootzen, W. Visscher, J.A.R. Van Veen, Langmuir 12 (1996) 5076.
[9] V.M. Schmidt, R. Ianniello, E. Pastor, S. Gonzalez, J. Phys. Chem. 100 (1996) 17901.
[10] J.P.I. de Souza, S.L. Queiroz, K. Bergamaski, E.R. Gonzalez, F.C. Nart, J. Phys. Chem. B 106 (2002) 9825.
[11] S.-C. Chang, L.-W.H. Leung, M.J. Weaver, J. Phys. Chem. 94 (1990) 6013.
[12] R. Sousa Jr., E.R. Gonzalez, J. Power Sources 147 (2005) 32.
[13] R. Sousa Jr., F. Colmati, E.R. Gonzalez, J. Power Sources 161 (2006) 183.
[14] Comsol AB, Comsol Multiphysics User's Guide, 1994–2005.
[15] S.V. Patankar, Numerical Heat Transfer and Fluid Flow, Hemisphere Publishing Corporation, USA, 1980.
[16] W.J. Minkowycz, Handbook of Numerical Heat Transfer, Wiley, New York, 1988.
[17] Comsol AB, Chemical Engineering Module User's Guide, 1994–2004.
[18] Comsol, Inc., http://www.comsol.com, 1997–2006.
[19] J. Norlund, G. Lindbergh, J. Electrochem. Soc. 149 (2002) A1107.
[20] S. Zhou, T. Schultz, M. Peglow, K. Sundmacher, Phys. Chem. Chem. Phys. 3 (2001) 347.
[21] K. Sundmacher, T. Schultz, S. Zhou, K. Scott, M. Ginkel, E.D. Gilles, Chem. Eng. Sci. 56 (2001) 333.
[22] T. Vidakovic, M. Christov, K. Sundmacher, J. Electroanal. Chem. 580 (2005) 105.
[23] B.E. Poling, J.M. Prausnitz, J.P. O'Connell, The Properties of Gases and Liquids, McGraw-Hill, New York, 2001.
[24] S. Kontou, N. Kaklidis, I. Koutla, S. Song, P. Tsiakaras, First European Fuel Cell Technology & Applications Conference, Rome, Italy, December 14–16, 2005.
[25] M. Bhattacharya, W.G. Devi, P.S. Mazumdar, Appl. Surf. Sci. 218 (2003) 1.
[26] J.X. Wu, Q.Y. Liu, J. Fuel Cell Sci. Technol. 2 (2005) 20.